International Journal of Mathematical Analysis and Modelling

(Formerly Journal of the Nigerian Society for Mathematical Biology)

Volume 7 Issue 1, 2024

ISSN (Print): 2682 - 5694
ISSN (Online): 2682 – 5708
www.tnsmb.org

Transient analysis of short circuit faults in hybrid networks

J.S. Zangina[*†], M.A. Suleiman[‡], and A. Ahmed[†§]

Abstract

Hybrid power systems, integrating renewable energy sources, energy storage devices, and conventional generators, are at the vanguard of the transition towards sustainable energy solutions. However, ensuring the robustness and reliability of these systems under fault conditions, particularly short circuit faults, remains a challenge. This research explores the complexity of hybrid networks, conducting a comprehensive transient analysis of short-circuit faults to enhance the understanding of their impact. The study employs advanced simulation techniques and state-of-the-art modeling approaches to examine the dynamic behavior of hybrid networks during fault events. Through detailed investigations, this research aims to unravel the transient responses of various fault locations, including fault resistance, and transmission line length, renewable energy sources, when subjected to short circuit faults. The findings of this study not only contribute to the academic discourse surrounding hybrid power systems but also provide invaluable insights for industry practitioners, guiding the development of reliable and efficient hybrid energy infrastructures for a sustainable future.

Keywords and phrases: First Fault resistance, hybrid power system, sustainable energy solution, transient analysis, transmission line

1 Introduction

Short-circuit analysis of a given power system is executed at the design stage to achieve optimum transformer system layout, conductor, and system voltage selection. Also, in the case of an existing power system, fault studies are essential in the events of system expansion and design of protection systems [1] – [3]. Various fault categories are present within power systems, broadly classified as symmetrical and unsymmetrical faults [4] – [8]. Determination of currents and voltage waveforms arising from various faults occurring at different locations within the power system network is essential [9], [10]. This information is crucial for designing an effective protective scheme, as highlighted in prior research [11] – [14]. It has been shown in [15] and [16] that the severity of the fault and its

[*]Corresponding Author; E-mail: jaafzangs@gmail.com
[†]Food and Industrial Biotechnology Department, National Biotechnology Development Agency, Abuja, Nigeria.
[‡]Software Engineering Department, Nile University of Nigeria, Abuja, Nigeria. E-mail: muhammad.suleiman @ nileuniversity.edu.ng
[§]Faculty of Engineering Science, Department of Electrical and Electronics Engineering, University of Nyala, Nyala, Sudan. E-mail: elamin2018@gmail.com

transient component in transmission systems depends on several factors, such as fault type, the magnitude of the system voltage at the instant of the fault occurrence, and fault location [17] – [19]. These factors significantly impact the shapes and amplitudes of voltage and current waveforms as well as the damping rates and frequencies across the transmission system.

The simulation of transient voltage and current, coupled with an analysis of diverse fault conditions that may arise during short circuit events, holds significant importance in the power system engineering practice. Transient overvoltage and current are widely recognized for inducing harmful thermal stress and fire hazards, potentially causing damage to power system equipment [20]. Short circuit on power system network is inevitable, but protective devices like circuit breakers and fuses should be able to cut off fault at a given location with considerable damage. Similarly, buses, cables, and disconnecting switches should be robust to withstand the mechanical and thermal stresses of short-circuit currents that flow through them [21], [22]. The selections of this equipment are subject to the magnitude of short circuit currents. The interaction of several apparatuses used for generating, transmitting, and distributing hybrid electrical power makes it somewhat of a complex system. The extreme complexity of these systems proposes ineluctable failures regardless of system perfection during the design stage. Rotating electrical machinery was considered the source of fundamental frequency currents that flow during a short circuit [23]. Power capacitors within the systems can also develop very high transient short-circuit discharge currents.

This research contributes to a deeper understanding of the dynamic behavior of hybrid power systems during short-circuit fault events. In particular, the study employs advanced simulation techniques that include numerical modeling, dynamic simulations, and state-of-the-art modeling approaches. These techniques are valuable in examining the complex transient phenomena during short-circuit faults in hybrid networks. The findings of this research offer practical guidance to industry practitioners involved in the design and operation of hybrid energy infrastructures. By understanding the transient behavior of these systems during short-circuit faults, practitioners can make informed decisions to enhance the reliability and efficiency of hybrid power systems. The work also contributes to the broader goal of creating a more sustainable and resilient energy infrastructure. It adds to the academic discourse surrounding hybrid power systems, which is critical in the perspective of global efforts to reduce greenhouse gas emissions and promote renewable energy. The research serves as a foundation for further studies in the field of fault analysis in hybrid networks. It provides a starting point for researchers to further explore the subject, investigate new fault scenarios, and develop mitigation strategies to enhance the robustness of hybrid power systems.

2 System description

The system comprises a conventional generation unit with a nominal capacity of 50MVA. The power system is outfitted with a synchronous generator connected via a hybrid transformer and a double-circuit line of 132 kV. The specific line configuration is illustrated in Fig. 1, with the total line length varying from 20 to 100 km. Detailed parameters are provided in Table 1.

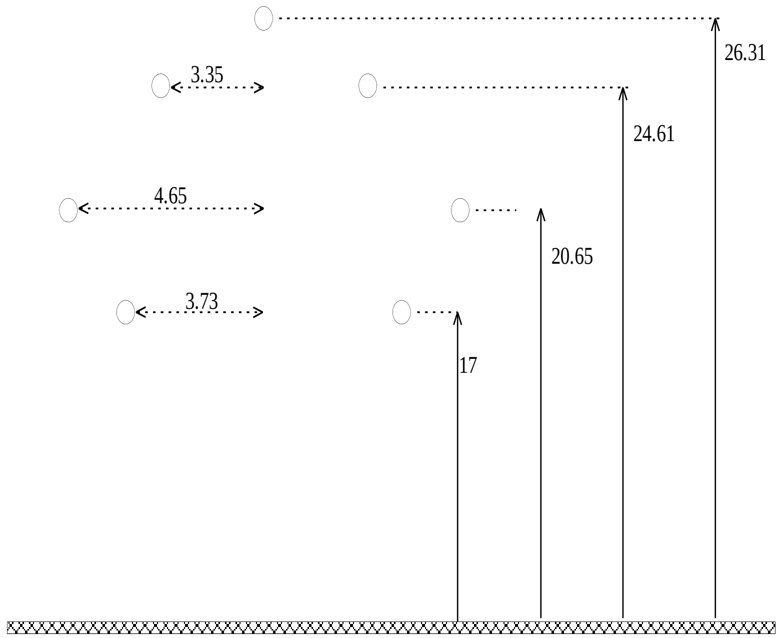

Fig. 1. Configuration of the overhead line (dimension in meters)

The transmission line is energized at one end by both conventional and wind generation, but in different locations, while the other end is open-circuited and on no-load.

Table 1. Details of the transmission line conductors

	Phase Conductor	Earth Wire
DC resistance (ohm/km)	0.156489	0.1469
Conductor radius (cm)	0.976	0.976
Number of conductors	1	1
Resistivity of the soil (Ω-m)	20	

2.1 Hybrid system configuration

Simulating transient voltages in a hybrid power network of transmission systems requires electromagnetic transient (EMT) simulation software. This simulation process is usually accompanied by time-consuming, which can hinder the efficiency of research and engineering tasks [24]. For this reason, it's essential to avoid unnecessary model assumptions and adopt a sufficient system model. It is imperative to recognize model elements with fast-front wave characteristics as they account for critical variables in the transient study. The hybrid power system component like transformer and generators in the ATPDraw program is suitable for a system with fast-front waves as it accounts for the magnetic saturation effects, main and leakage flux losses, and coil capacitances [25]. These variables are essential in power system transient study. The wind farm model from the ATPDraw Windsyn is employed to complete the hybrid power system setup. The Windsyn control mechanism operates to maintain more than 0.89 lagging power factor at the terminal bus of the wind farm. The nominal power generation of the wind farm is 35 MW. The equivalent diagram of the system is shown in Fig. 2.

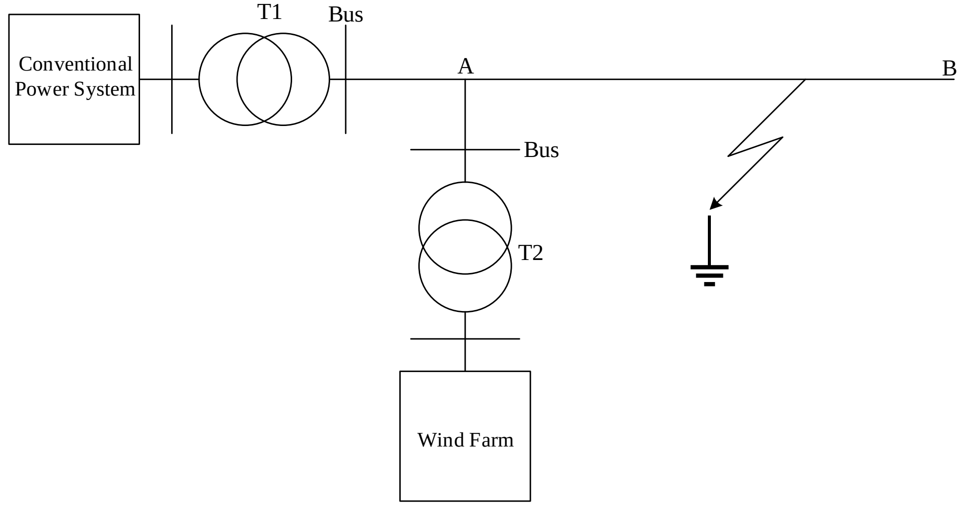

Fig. 2. Single line equivalent diagram of the hybrid power system

2.2 Transmission Line Model

To accurately model the transmission line for the transient study, a frequency-dependent distributed line mode is adopted. Consider a small portion of the long segment of the line as shown in Fig. 3. Let the total line be x and a small segment of it Δy, then the wave propagation along the line is described as follows:

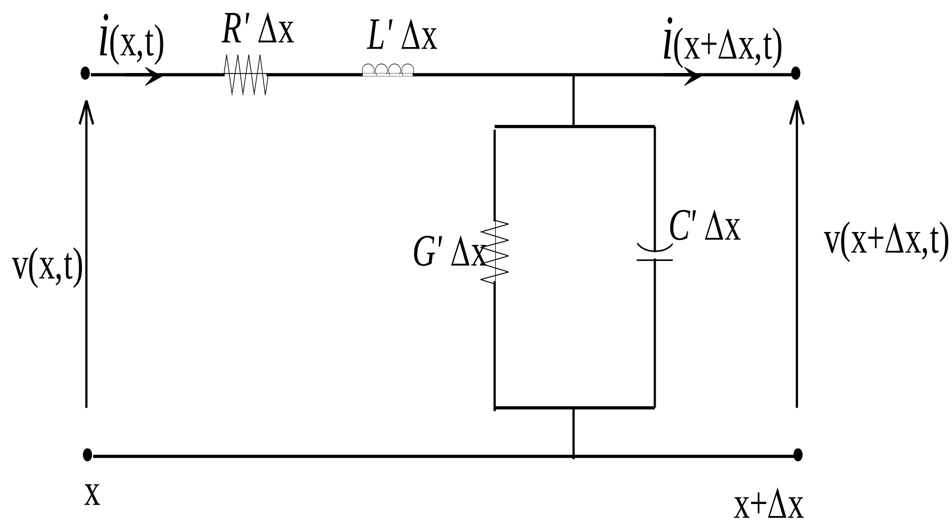

Fig. 3. Transmission line segment

$$\frac{\partial i}{dy} = -vG' - \frac{\partial v_o}{\partial t}C' \tag{1}$$

$$\frac{\partial v}{\partial y} = -iR' - \frac{\partial i_i}{\partial t}L' \tag{2}$$

where R' is the transmission line resistance in Ω/km, L' denote inductance in H/km, C' is the capacitance in F/km, G' denote the shunt conductance in Ω-1/km.

$$\frac{\partial^2 v}{\partial y^2} = -R'\frac{\partial i}{\partial y} - L'\frac{\partial^2 i}{\partial y \partial t} \quad (3)$$

$$\frac{\partial^2 v}{\partial y \partial t} = -R'\frac{\partial i}{\partial t} - L'\frac{\partial^2 i}{\partial t^2} \quad (4)$$

$$\frac{\partial^2 i}{\partial y \partial t} = -G'\frac{\partial v}{\partial t} - C'\frac{\partial^2 v}{\partial t^2} \quad (5)$$

$$\frac{\partial^2 i}{\partial y^2} = -G'\frac{\partial v}{\partial t} - L'\frac{\partial^2 v}{\partial y \partial t} \quad (6)$$

$$\frac{\partial^2 v}{\partial y^2} = v(R'G') + \frac{\partial v}{\partial t}(L'G' + R'C') + (C'L')\frac{\partial^2 v}{\partial t^2} \quad (7)$$

$$\frac{\partial^2 i}{\partial y^2} = i(R'G') + \frac{\partial i}{\partial t}(L'G' + R'C') + (C'L')\frac{\partial^2 i}{\partial t^2} \quad (8)$$

$$\frac{\partial^2 v}{\partial y^2} = v(R'G') + j\omega v(y,t)(L'G' + R'C') - (C'L')\omega^2 v(y,t) \quad (9)$$

$$\frac{\partial^2 v}{\partial y^2} = v(y,t)[(R + j\omega L)(G + j\omega C)] \quad (10)$$

$$v(y) = K_0 e^{-\gamma y} + K_1 e^{\gamma y} \quad (11)$$

$$\gamma = \sqrt{[(R' + j\omega L')(G' + j\omega C')]} \quad (12)$$

where γ is the propagation constant, ω represents angular velocity.

The current wave propagation along the line and the characteristics impedance becomes:

$$i(y,t) = \frac{-\gamma K_0 e^{-\gamma y} + \gamma K_1 e^{\gamma y}}{(R' + j\omega L')} \quad (13)$$

$$\frac{v(y,t)}{i(y,t)} = Z_0 \quad (14)$$

$$Z_0 = \sqrt{\frac{R' + j\omega L'}{G' + j\omega C'}} \quad (15)$$

However, in the case of frequency-dependent factors, the wave propagation characterized by impedance and propagation constant is determined by the following expression:

$$Z_c(\omega) = \sqrt{\frac{R'(\omega) + j\omega L'(\omega)}{G'(\omega) + j\omega C'(\omega)}} \quad (16)$$

$$Z_c(\omega) = \sqrt{\frac{Z'(\omega)}{Y'(\omega)}} \quad (17)$$

where $Z'(\omega)$ is the series impedance matrix, $Y'(\omega)$ is the shunt admittance matrix.
The fault in a power system is known to cause distortion in the current and voltage waveform along the transmission line. This fault can be represented by the equations, which describe the relationship between voltage and current along the line:

$$V(x) = V_{in}e^{-\gamma x} + V_r e^{\gamma x} \quad (18)$$

$$I(x) = \frac{V_{in}}{Z_0}e^{-\gamma x} - \frac{V_r}{Z_0}e^{\gamma x} \quad (19)$$

where $V(x)$ is the voltage at a distance x along the line, $I(x)$ is the current at a distance x, V_{in} denotes incident voltage at the beginning of the line, V_r denotes a reflected voltage wave caused by a fault.

3 Result and discussion

Consider the short circuit fault on a single phase at the transmission line end (point A) when the phase voltage is at the peak value. The Maximum values of the sending-end faulted phase current for different line lengths are given in Table 2. The simulation result shows that the maximum magnitude of the sending end currents increases as the line length increases. Also, the observed ripples along the line attenuate as the line length increases. The faulted phase sending-end currents during fault are computed for various line lengths and plotted to obtain faulted phase current waveform as shown in Fig. 4a and 4b, respectively.

Table 2. Table captions should be placed above the tables.

Distance between fault point and the first sending-end of the line (km)	Maximum magnitude of the first sending-end current (A)
20	249.42
40	353.39
60	397.19
80	408.02

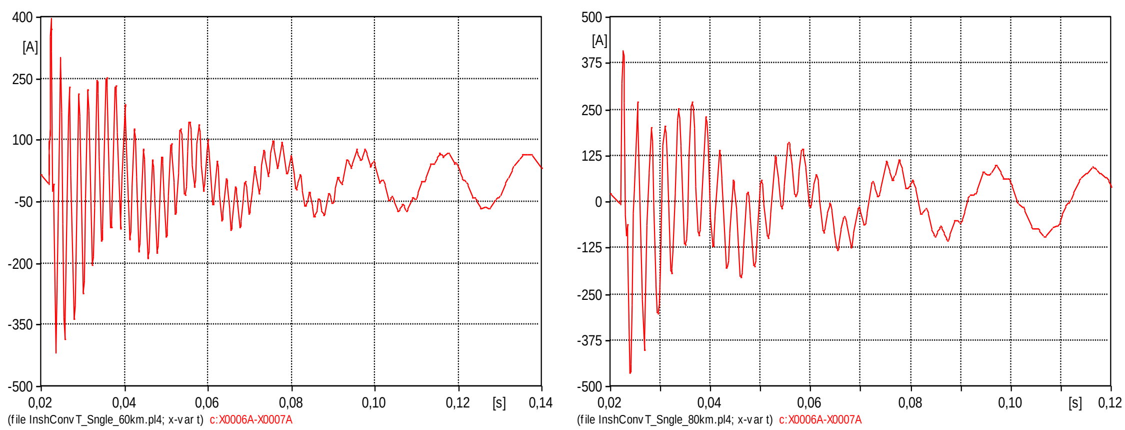

Fig. 4. Sending-end faulted phase current on the line at (a) 60km, (b) 80km.

The sending-end unfaulted phase voltages waveform is shown in Fig. 5a and 5b for 40 and 100km, respectively. It is observed from the result that as the line length increases, the unfaulted phase voltages decrease, and likewise, the distortion also decreases.

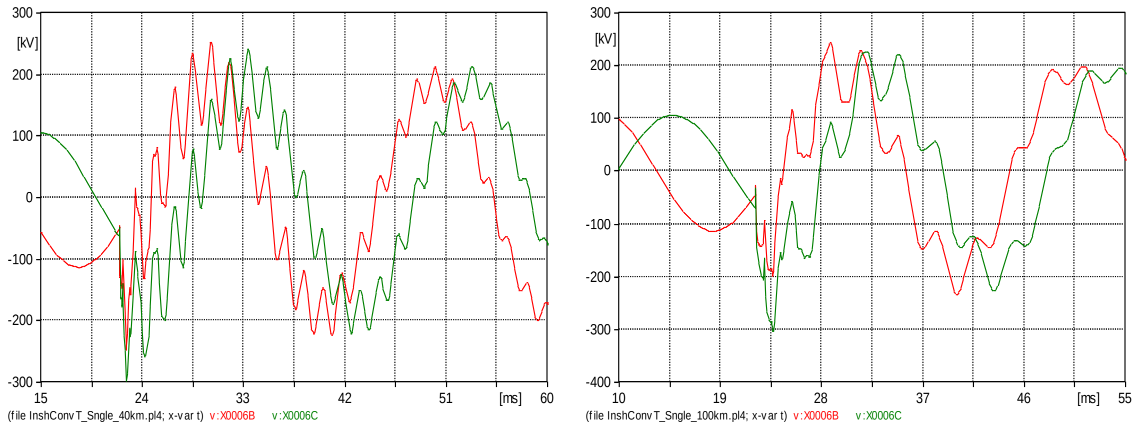

Fig. 5. Sending-end unfaulted phase voltages for the line at (a) 40 km, (b) 100km.

A single-phase to-earth fault is considered to occur at the receiving end of the line during fault resistance, as shown in Fig 6. The earth fault is assumed to occur when the voltage of the faulted phase is at its peak value. When an earth fault happens, it often causes a sudden increase in current flow through the grounding system. Detecting and addressing earth faults promptly is crucial because they can lead to equipment damage, electrical fires, or even pose a risk to human safety. One common method used to identify earth faults is by monitoring the voltage of the faulted phase.

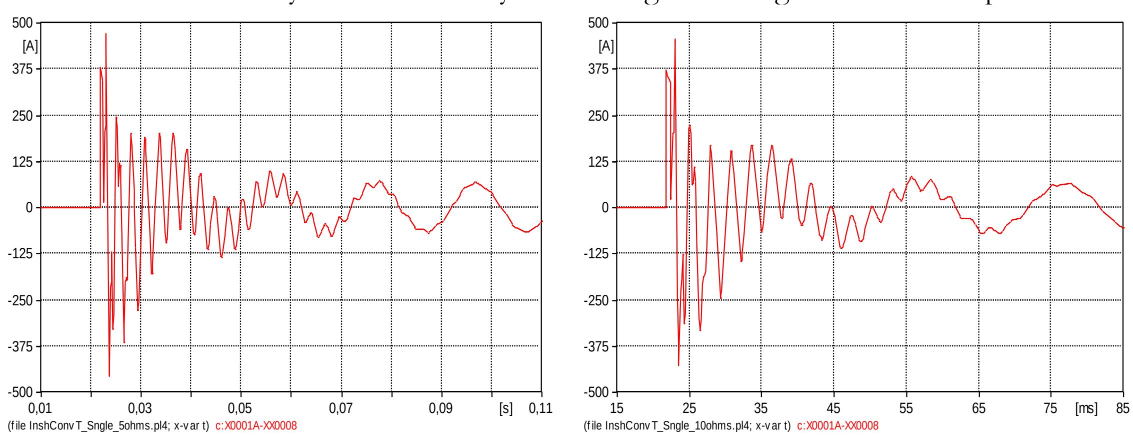

Fig. 6. Fault current at the fault location fault resistance (a) 5 ohms, (b) 10 ohms.

Variation of maximum fault currents at the sending end and the fault location for different fault resistances is given in Table 3. The maximum magnitude of fault currents at the sending-end and fault location decreases as the fault resistance increases. The distortion in the fault current waveform is higher at a lower value of the fault resistance as compared to that of a higher value.

Table 3. Variation of maximum sending-end faulted phase current and maximum magnitude fault current at fault location against fault resistance.

Fault resistance (ohms)	Maximum magnitude of first sending-end current (A)	Maximum magnitude fault current at fault location (A)
1	406.59	485.22
5	400.97	472.33
10	394.16	457.10
20	381.17	429.28
50	346.94	362.64

Double-phase to-earth and three-phase to-earth faults are considered. The fault occurs at the receiving end of the line on phases B and C in the case of a double-phase fault. The maximum magnitude of the fault current at the fault location is recorded. Similarly, in the case of three-phase-to-earth fault simulation, currents and voltages computed were also taken at the fault and sending-end points, respectively. For a double phase-to-earth fault, waveforms of faulted phase currents at the sending end are given in Fig. 7a. Similarly, Fig. 7b depicts the faulted phase current during a three-phase fault at the sending end. However, the three-phase faulted waveforms for the faulted phases A, B, and C voltage at the sending end, and the faulted phase currents at the fault location are given in Fig. 8a and 8b, respectively. This information aids in the design and setting of protective devices such as circuit

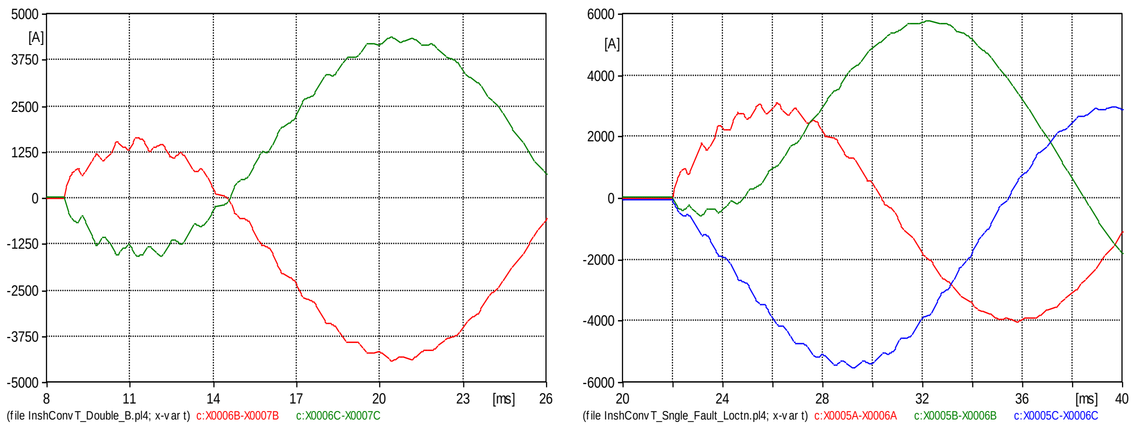

Fig. 7. Faulted phase currents at the sending-end (a) Double phase (b) Three phase.

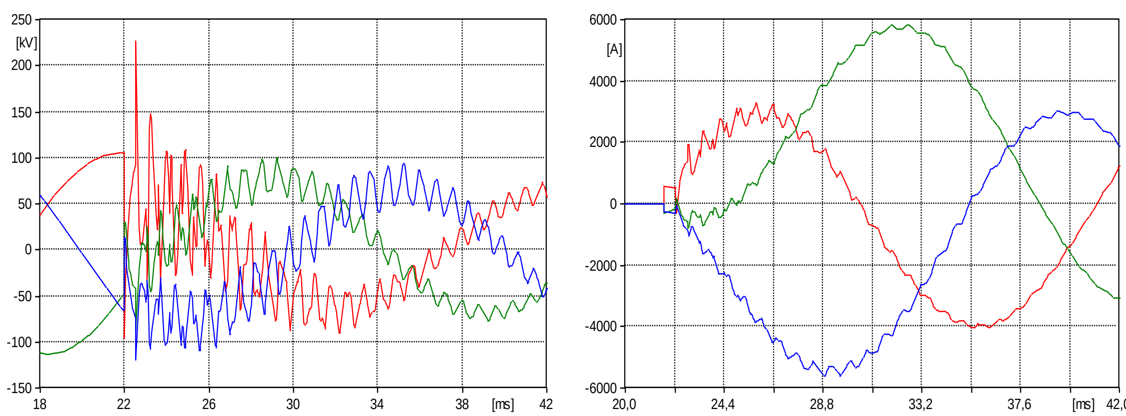

Fig. 8. Faulted phases (a) voltages at the sending-end, (b) currents at the fault location

breakers and relays. Understanding the variation of fault currents against fault resistance helps in the selection of appropriate protection settings to isolate the faulty section quickly, preventing extensive damage to the equipment.

This study investigates transient voltage and over-current responses arising from various fault conditions within a power system. The findings confirm that the severity of fault transients in the examined power system is contingent upon several factors, including fault type, line length, fault location, and the system voltage magnitude at the moment of the fault occurrence. These variables influence the amplitudes and shapes of current and voltage waveforms along the transmission system. The analysis of the waveforms reveals that an increase in line length or fault resistance correlates with the distortion reduction within the current waveforms. Moreover, voltage waveforms exhibit higher amplitude and frequency oscillations than the current waveforms. During a three-phase fault to ground occurring at the line's end, voltage waveforms display substantial instability characterized by high amplitudes, distinguishing them from other fault types. Similarly, transient fault currents recorded at the fault location surpass those at any other point within the transmission system.

4 Conclusion

The analysis conducted in this study plays a fundamental role in the strategic planning, design, and operation of hybrid power systems. Voltage and current data collected during various fault scenarios serve as crucial inputs for devising the protective framework, comprising protective relays, switch gears, and circuit breakers. Notably, this research focuses explicitly on assessing the impact of short circuit faults on hybrid power systems.

A distinctive feature of this study lies in its explicit focus on the short circuit faults assessment within hybrid power systems. Through rigorous analysis and meticulous experimentation, the research sheds light on the intricate dynamics of these faults, unraveling their impact on the stability and reliability of hybrid power setups. This insight is invaluable, guiding future endeavors in the field and providing a solid foundation for advanced protective strategies. In essence, this study not only contributes to the academic discourse but also holds immense practical implications for the broader energy landscape. By continually refining our understanding of hybrid power system behavior, we move closer to a future where clean and reliable energy is readily accessible, paving the way for a more sustainable world.

References

[1] Zhuang, S., Miao, X., Lin, Y., and Liu, Q. (2024). The early detection of short-circuit fault in the active low-voltage AC system. Int. J. Electr. Power Energy Syst., 155: 109476.

[2] Taheri, B., Salehimehr, S., and Sedighizadeh, M. (2022). A novel strategy for fault location in shunt-compensated double circuit transmission lines equipped by wind farms based on long short-term memory. Cleaner Eng. Technol., 6: 100406.

[3] Pascoalato, T. F. G., de Araújo, A. R. J., Kurokawa, S., and Filho, J. P. (2023). Alternative method to include the frequency-effect on transmission line parameters via state-space representation.

Int. J. Electr. Power Energy Syst., x: 109375.
[4] Topolanek, D., Krcal, V., Foltyn, L., Praks, P., Vysocky, J., Praksova, R., Prettico, G., and Fulli, G. (2023). Optimization method for short circuit current reduction in extensive meshed LV network. Int. J. Electr. Power Energy Syst., 152: 109203.
[5] Zheng, Z., Li, Q., Li, X., Zheng, P., Wang, K., and Cui, P. (2022). Analysis and fault-tolerant control of inter-turn short-circuit fault for five-phase permanent-magnet synchronous machine. Energy Rep., 8: 7360–7373.
[6] Xiao, F., Xia, Y., Zhang, K., Zhang, Z., and Yin, X. (2022). Short-circuit model of the DFIG considering coordinated control strategy of grid- and rotor-side converters. Energy Rep., 8: 1046–105.
[7] Yin, J. (2021). Influence of reactive power support control strategy on short-circuit current calculation and fault analysis method of DFIG. Energy Rep., 7: 5933–5942.
[8] Murzintseva, A., Korolev, A., Zhgun, K., and Baembitov, R. (2020). Short-circuit Current reduction in auxiliary network of traction substation. Transp. Res. Procedia., 54: 346–354.
[9] Lacerda, V. A., Araujo, E. P., Chea-Mañe, M., and Gomis-Bellmunt, O. (2023). Phasor and EMT models of grid-following and grid-forming converters for short-circuit simulations. Electric Power Syst. Res., 223: 109662.
[10] Mishra, S. K., Tripathy, L. N., and Swain, S. C. (2019). DWT approach based differential relaying scheme for single circuit and double circuit transmission line protection including STATCOM. Ain Shams Eng. J., 10: 93-102.
[11] Amin, A., Abdelaziz, A. Y., Attia, M. A., and Kamh, M. Z. (2023). Optimal reconfiguration for Extra high voltage transmission networks using an enhanced Brute-Force algorithm. Ain Shams Eng. J., X: 102246
[12] Teng, Z., Chen, W., Zhaoa, J., Zhang, J., Gan, Z., and Li, K. (2022). Measurement of electromagnetic environment of hybrid DC circuit breaker during bipolar short circuit fault. Energy Rep., 8: 1328–1335.
[13] Abdulkareem, Adesanya, A., Agbetuyi, A. F., and Alayande, A. S. (2021). Novel approach to determine unbalanced current circuit on Nigerian 330kV transmission grid for reliability and security enhancement. Heliyon, 7: e07563.
[14] Ding, C., Tian, X., Nie, T., and Yuan, Z. (2020). Influence of capacitor-buffered hybrid DC circuit breaker on bipolar short circuit fault of three-terminal MMC-HVDC transmission system. Energy Rep., 6: 1276–1282.
[15] Daisy, M., Aliabadi, M. H., Javadi, S., and Naimi, H. M. (2023). A robust transient and sustainable faults location approach for AC microgrid based on voltage and current difference measurements. Int. J. Electr. Power Energy Syst., 153: 109343.
[16] Song X., Feng T., Han, L., Smith, T. M., Dong, X., Liu, W., and Zhang, R. (2018). Analysis on the fault characteristics of three-phase short-circuit for half-wavelength AC transmission lines. Glob. Energy Intercon., 1: 115-121.
[17] Pinchukov, P. and Makasheva, S. (2023). Harmonic Monitoring in Normal and Short-Circuit Modes of AC Traction Network. Transport. Res. Procedia 68: 980–986.
[18] Liu, Y., Lu, D., Vasilev, S., Wang, B., Lu, D., and Terzija, V. (2023). Model-based transmission line fault location methods: A review. Int. J. Electr. Power Energy Syst., 153:109321.
[19] Zhang, Y., Zhanga, Y., Pan, X., Zhao, B., He, J., Han, Y., Zhang, J., Wang, X., Yu, Z., Bu, G., and Ye, J. (2022). Equivalent modeling method of induction motor contribution to short-circuit current. Energy Rep., 8:1202–1210.
[20] Qi, S., Chang, S., and Cao, L. (2021). Transient discharge characteristics of insulator short-circuit

under high voltage. Alex. Eng. J. 60: 5175-5181.

[21] Zhang, T., and Wang, N. (2023). Transmission line fault classification based on spatiotemporal characteristic analysis with global and local discriminant analysis. Eng. Sci. Technol. Int. J., 45: 101476.

[22] Treider, T. and Høidalen, H. K. (2023). Estimating distance to transient and restriking earth faults in high-impedance grounded, ring-operated distribution networks using current ratios. Electric Power Syst. Res., 224: 109765.

[23] E. Muljadi, N. Samaan, V. Gevorgian,; J. Li; S. Pasupulati, "Short Circuit Current Contribution for Different Wind Turbine generator Types" Proc. IEEE PES Gen. Meeting, 1-8.

[24] Khalilnezhad, H., Popov, M., van der Sluis, L., Bos, J. A., and Ametani, A. (2018). Statistical analysis of energization overvoltages in EHV hybrid OHL–cable systems, IEEE Trans. Power Del., 33: 2765–2775.

[25] Høidalen, H. K., Mork, B. A., Gonzalez, F., Ishchenko, D., and Chiesa, N. (2007) "Implementation and verification of the Hybrid Transformer model in ATPDraw" IPST., 4-7.